

PACS numbers: 52.38.–r; 52.25.–b; 52.50.Jm
DOI: 10.1070/QE2006v036n02ABEH00

Mathematical simulation of the spectrum of a nonequilibrium laser plasma

V.I. Mazhukin, M.G. Nikiforov, Ch. Fievet

Abstract. **A method is proposed for calculating the spectrum of a nonequilibrium plasma, which is based on a nonequilibrium collision–radiation model including all common line broadening mechanisms (natural, pressure, Doppler, and quadratic Stark effect broadening) and supplemented with the energy balance equations for electrons and ions. The nonequilibrium populations of the ground and excited states of neutral atoms and ions for an arbitrary instant of time are found by solving kinetic equations. The shape of each spectral line is determined by its central core calculated in the collision approximation up to the frequency boundary of its applicability, where the central core is 'joined' with the line wings calculated in the quasi-static approximation. The validity of this theoretical model is confirmed by simulations of a number of experimental studies of emission spectra under the conditions of a local thermodynamic equilibrium. It is shown that the calculated and experimental data obtained for the ground-state lines of the first carbon ion and neutral helium and argon atoms are in good agreement. The nonequilibrium spectrum of the optical breakdown in argon is calculated. Mathematical simulations showed that the intensities of nonequilibrium line spectra can be noticeably (by several times) lower than those of equilibrium spectra.**

Keywords: nonequilibrium laser plasma, line spectrum, broadening mechanisms, kinetic model.

1. Introduction

Spectroscopy plays an important role in the methods for plasma diagnostics, allowing one to study and analyse processes proceeding in a plasma and to measure the plasma temperature, charge composition, and concentrations of particles. There exist various spectroscopic methods for measuring the plasma temperature such as the method of brightness distribution in a continuum [1], method of comparing brightness of two continua [2], method of the relative intensities of spectral lines [3], and the measurement of temperature from the spectral line shape [4].

V.I. Mazhukin, M.G. Nikiforov Institute of Mathematical Modelling, Russian Academy of Sciences, Miusskaya pl. 4a, 125047 Moscow, Russia; e-mail: immras@orc.ru
Ch. Fievet Schneider Electric Research Centre A2, 38050 Grenoble Cedex, France

Received 19 May 2005; revision received 27 October 2005
Kvantovaya Elektronika 36 (2) 125–133 (2006)
Translated by M.N. Sapozhnikov

However, all these methods have a limited field of applications. First, they are based on the assumption of a local thermodynamic equilibrium, which requires the additional substantiation of their application for nonequilibrium processes. The first and second methods [1, 2] are commonly used at sufficiently high temperatures, when the intensity of bremsstrahlung and recombination emission spectra is high. The third method assumes the presence of the Saha–Boltzmann equilibrium, while the fourth method requires the absence of self-absorption in a line, which substantially restricts the field of its applications.

Thus, neither of these methods is universal for plasma diagnostics. A comparison of the experimental characteristics of a plasma with the results of its mathematical simulation successfully supplements the known methods for plasma diagnostics. For this purpose, we developed the nonequilibrium collision–radiation kinetic model describing the interaction of radiation with matter and supplemented with various line broadening mechanisms.

2. Nonequilibrium collision-radiation kinetic model

2.1 Population and ionisation kinetics

In a gas medium interacting with laser radiation, a variety of different elementary reactions occur, which determine together the character of a macroprocess. Our model and calculations are based on the following assumptions:

(i) the atomic plasma of one chemical element is considered;

(ii) a substance is initially in the thermodynamically equilibrium state;

(iii) the plasma is spatially homogeneous, i.e., its temperature and density are spatially invariable.

The collision–radiation kinetic model includes many excited states of emitting atoms and ions. To each state the ordinary differential equation corresponds, which describes the balance of particles coming to and leaving the level due to elementary microprocesses. The realised collision–radiation model includes ten elementary processes (reactions) presented in Table 1.

Taking into account the data on characteristic rates of processes, the system of kinetic equations for the ground and excited states of neutral atoms and ions can be written in the form

$$\frac{\mathrm{d}N_0^0}{\mathrm{d}t} = -\sum_{j=1}^{M_0}\left(k_{0j}^0 N_0^0 - r_{j0}^0 N_j^0\right)N_\mathrm{e} - \left(\alpha_0^0 N_0^0 - \beta_0^0 N_0^1 N_\mathrm{e}\right)N_\mathrm{e} +$$

Table 1.

Process number	Elementary process	Process frequency (probability)/ s^{-1}	Process rate
1	Spontaneous decay		
	$N_n^z \xrightarrow{A_{nm}^z} N_m^z + \hbar\omega_{nm}^z$	A_{nm}^z	
2	Collision excitation/decexcitation		k_{nm}^z, r_{nm}^z/ $cm^3\ s^{-1}$
	$N_m^z + c \xrightarrow[r_{nm}^z]{k_{nm}^z} N_n^z + e$		
3	Electron impact ionisation		α_m^z/ $cm^3\ s^{-1}$
	$N_m^z + c \xrightarrow{\alpha_m^z} N_0^{z-1} + 2e$		
4	Three-body recombination		β_m^z/ $cm^6\ s^{-1}$
	$N_0^{z+1} + 2c \xrightarrow{\beta_m^z} N_m^z + c$		
5	Laser photoionisation		
	$N_m^z + \hbar\omega_\lambda \xrightarrow{{}^\lambda\nu_m^z} N_0^{z+1} + e$	${}^\lambda\nu_m^z$	
6	Recombination in the laser radiation field		${}^\lambda R_m^z$/ $cm^3\ s^{-1}$
	$N_0^{z+1} + c + \hbar\omega_\lambda \xrightarrow{{}^\lambda R_m^z} N_m^z + \hbar\omega$		
7	Ionisation by continuous radiation		
	$N_m^z + \hbar\omega_c \xrightarrow{{}^c\nu_m^z} N_0^{z+1} + e$	${}^c\nu_m^z$	
8	Recombination in the continuous radiation field		${}^cR_m^z$/ $cm^3\ s^{-1}$
	$N_0^{z+1} + c + \hbar\omega_c \xrightarrow{{}^cR_m^z} N_m^z + \hbar\omega_c$		
9	Laser excitation		
	$N_m^z + \hbar\omega_\lambda \xrightarrow{{}^\lambda\nu_{nm}^z} N_n^z$	${}^\lambda\nu_{nm}^z$	
10	Excitation by continuous radiation		
	$N_m^z + \hbar\omega_c \xrightarrow{{}^c\nu_{nm}^z} N_n^z$	${}^c\nu_{nm}^z$	

Notes: N_n^z is the ion with the charge z in the state n; $\hbar\omega_{nm}^z$ is the $m-n$ transition energy; $\hbar\omega_\lambda$ is the laser radiation photon; $\hbar\omega_c$ is the continuous radiation photon; A_{nm}^z is the probability of spontaneous decay of the excited state n to the state m; k_{nm}^z and r_{nm}^z are the rates of the electron-impact excitation and deexcitation of the N_m^z ion; α_m^z is the electron-impact ionisation of the N_m^z ion from the state m; β_m^z is the coefficient of three-body recombination of the N_m^z ion; ${}^\lambda\nu_m^z$ and ${}^c\nu_m^z$ are the frequencies of photoionisation of the N_m^z ion in the fields of laser and continuous radiation, respectively; ${}^\lambda R_m^z$ and ${}^cR_m^z$ are the coefficients of photorecombination of the N_0^{z+1} ion in the fields of laser and continuous radiation, respectively; ${}^\lambda\nu_{nm}^z$ and ${}^c\nu_{nm}^z$ are the excitation frequencies of the N_m^z ion by laser and continuous radiation, respectively.

$$+\sum_{j=1}^{M_0} A_{j0}^0 N_j^0 - \sum_{j=1}^{M_0} {}^c\nu_{0j}^0\left(N_0^0 - \frac{g_0}{g_j} N_j^0\right)$$

$$-\sum_{j=1}^{M_0} {}^\lambda\nu_{0j}^0\left(N_0^0 - \frac{g_0}{g_j} N_j^0\right) - \left({}^\lambda\nu_0^0 + {}^c\nu_0^0\right)N_0^0$$

$$+\left({}^cR_0^0 + {}^\lambda R_0^0\right)N_0^1 N_e \qquad (1)$$

for the ground state of neutral atoms ($z = 0$);

$$\frac{dN_0^z}{dt} = -\sum_{j=1}^{M_z}\left(k_{0j}^z N_0^z - r_{j0}^z N_j^z\right)N_e + \sum_{j=0}^{M_{z-1}}\left(\alpha_j^{z-1} N_j^{z-1} - \beta_j^{z-1} N_0^z N_e\right)N_e - \left(\alpha_0^z N_0^z - \beta_0^z N_0^{z+1} N_e\right)N_e$$

$$+\sum_{j=1}^{M_z} A_{j0}^z N_j^z - \sum_{j=1}^{M_z} {}^c\nu_{0j}^z\left(N_0^z - \frac{g_0^z}{g_j^z} N_j^z\right)$$

$$-\sum_{j=1}^{M_z} {}^\lambda\nu_{0j}^z\left(N_0^z - \frac{g_0^z}{g_j^z} N_j^z\right) - \left({}^c\nu_0^z + {}^\lambda\nu_0^z\right)N_0^z$$

$$+\left({}^cR_0^z + {}^\lambda R_0^z\right)N_0^{z+1} N_e + \sum_{n=0}^{M_{z-1}}\left({}^c\nu_n^{z-1} + {}^\lambda\nu_n^{z-1}\right)N_n^{z-1}$$

$$-\sum_{n=0}^{M_z}\left({}^cR_n^{z-1} + {}^\lambda R_n^{z-1}\right)N_0^z \qquad (2)$$

for the ground state of ions with the charge $z \in (1, 2, \ldots, z_{max} - 1)$;

$$\frac{dN_m^z}{dt} = \sum_{j=0}^{m-1}\left(k_{jm}^z N_j^z - r_{mj}^z N_m^z\right)N_e - \sum_{j=m+1}^{M_z}\left(k_{mj}^z N_m^z - r_{jm}^z N_j^z\right)N_e$$

$$-\left(\alpha_m^z N_m^z - \beta_m^z N_0^{z+1} N_e\right)N_e + \sum_{j<m}^{M_z} {}^c\nu_{jm}^z\left(N_j^z - \frac{g_j^z}{g_m z} N_m^z\right)$$

$$-\sum_{j>m}^{M_z} {}^c\nu_{mj}^z\left(N_m^z - \frac{g_m^z}{g_j^z} N_j^z\right) + \sum_{j<m}^{M_z} {}^\lambda\nu_{jm}^z\left(N_j^z - \frac{g_j^z}{g_m^z} N_m^z\right)$$

$$-\sum_{j>m}^{M_z} {}^\lambda\nu_{mj}^z\left(N_m^z - \frac{g_m^z}{g_j^z} N_j^z\right) - \sum_{j=0}^{m-1} A_{mj}^z N_m^z + \sum_{j=m+1}^{M_z} A_{jm}^z N_j^z -$$

$$-\left({}^c\nu_m^z + {}^\lambda\nu_m^z\right)N_m^z + \left({}^cR_m^z + {}^\lambda R_m^z\right)N_0^{z+1} N \qquad (3)$$

for the excited states of neutral atoms and ions ($m = 1, 2, \ldots, M_z$, $z = 0, 1, 2, \ldots, z_{max} - 1$);

$$\frac{dN_0^{z^*}}{dt} = \sum_{j=0}^{M_{z^*-1}}\left(\alpha_j^{z^*-1} N_j^{z^*-1} - \beta_j^{z^*-1} N_0^{z^*} N_e\right)N_e \qquad (4)$$

$$+\sum_{n=1}^{M_{z^*-1}}\left[\left({}^c\nu_n^{z^*-1} + {}^\lambda\nu_n^{z^*-1}\right)N_n^{z^*-1} - \left({}^cR_n^{z^*-1} + {}^\lambda R_n^{z^*-1}\right)\right]N_0^{z^*} N_e$$

for the concentration of ions with the charge $z = z^* = z_{max}$; and

$$\frac{dN_e}{dt} = \sum_{z=1}^{z_{max}}\sum_{m=0}^{M_z}\frac{dN_m^z}{dt} \qquad (5)$$

for the electron concentration. Here, N_m^z is the density of ions with the charge z in the state m; g_m^z is the static weight; N_e is the density of free electrons; M_z is the number of excited states of ions with the charge z included into the model; and z_{max} is the maximum degree of ionisation of a neutral atom. It is assumed that an ion with the maximum degree of ionisation has no spectral structure, i.e., its excited states are neglected.

2.2 Energy balance

An external electromagnetic radiation field incident on an absorbing medium (partially ionised gas, plasma) removes it from the equilibrium state. Processes of excitation, ionisation, recombination, and photoemission tend to bring the state of the absorbing medium to the correspondence with an external energy source, i.e., to establish a

new equilibrium. Taking into account that the characteristic relaxation times of the involved kinetic processes substantially differ from each other (by a few orders of magnitude), the system of kinetic equations is traditionally attributed to the so-called rigid systems. The relaxation of a plasma occurs as a whole in a complicated way and is determined by the time of the slowest process. In a plasma or partially ionised gas, three energy subsystems can exist in which the local equilibrium is established much rapidly than the energy exchange between them. These are subsystems whose properties are determined by the translation energy of atoms and ions and the total internal energy of excited atoms and molecules. The latter depends on the densities of electrons, atoms, and ions and is usually not written explicitly in equations.

The energy balance of the translational degrees of freedom is described by two equations for energy with a common exchange term. The electron and ion temperatures T_e and T_i are found from their simultaneous solution. The mechanism of the electromagnetic field energy transfer to free electrons substantially depends on the laser radiation wavelength. The electron energy balance in the IR region is determined by the energy of elastic collisions of electrons with atoms and ions (inverse bremsstrahlung effect) and is supplemented with the energy released during relaxation and recombination.

The energy of laser radiation in the visible and UV regions becomes comparable with the ionisation energy of excited states and the influence of inverse bremsstrahlung effect rapidly decreases. In this case, photoprocesses begin to play an important role in the energy balance of free electrons. The energy losses in the electron subsystem are mainly caused by inelastic processes (electronic excitation and ionisation) and quasi-elastic collisions accompanied by energy transfer between atoms and molecules. The translational energy of atoms and ions is completely determined by energy exchange with the electron subsystem.

Equations for the energy of translational degrees of freedom of electrons and heavy particles are written in the form [5, 6]

$$\frac{3}{2}\frac{\mathrm{d}(N_e T_e)}{\mathrm{d}t} = \left[\mu G - \frac{3}{2}\delta(T_e - T_i)\right](\nu_{en} + \nu_{ei})N_e - \sum_{z=0}^{z^*-1}\sum_{m=0}^{M_z} Q^z_{mJ} - \sum_{z=0}^{z^*-1}\sum_{m=0}^{M_z} Q^z_{m\Delta E} + \sum_{z=0}^{z^*-1} Q^z_{m\Phi}, \tag{6}$$

$$\frac{3}{2}\frac{\mathrm{d}(N_i T_i)}{\mathrm{d}t} = \frac{3}{2}\delta(T_e - T_i)(\nu_{en} + \nu_{ei})N_e, \tag{7}$$

where

$$\mu = \frac{4\pi e^2}{m_e c\left[\omega^2 + (\nu_{en} + \nu_{ei})^2\right]};\quad \delta = \frac{2m_e}{M_a};\quad N_i = \sum_{z=0}^{z_{max}}\sum_{m=0}^{M_z} N^z_m;$$

$$Q^z_{m\Delta E} = \sum_{j=m+1}^{M_z} E^z_{jm}(k^z_{mj}N^z_m - r^z_{jm}N_j)N_e;$$

$$Q^z_{mJ} = J^z_m(\alpha^z_m N^z_m - \beta^z_m N_0^{z+1}N_e)N_e;$$

$$Q^z_{m\Phi} = \sum_{m=0}^{M_z}\left[(\hbar\omega_\lambda - J^z_m)\left({}^{\lambda}\nu^z_m N^z_m - {}^{\lambda}R^z_m N_e N_0^{z+1}\right) + (\hbar\omega_c - J^z_m)\left({}^{c}\nu^z_m N^z_m - {}^{c}R^z_m N_e N_0^{z+1}\right)\right];$$

G is the laser radiation intensity; ν_{en} and ν_{ei} are the frequencies of electron–atom and electron–ion collisions; $Q^z_{m\Delta E}$, Q^z_{mJ}, and $Q^z_{m\Phi}$ are the specific powers characterising the energy exchange due to inelastic collisions, ionisation–recombination, and photoionisation–photorecombination, respectively; N_i is the ion concentration; e is the electron charge; m_e is the electron mass; M_a is the atom mass; E^z_{jm} is the energy of transition between the j and m levels of the ion with the charge z; and J^z_m is the ionisation potential of the m state of the ion with the charge z.

The system of differential equations (1)–(7) is supplemented with the corresponding initial conditions ($t = 0$)

$$N_0(0) = N_0^0,\ N_m(0) = N_m^0,\ N_e(0) = N_i(0) = N_e^0,$$

$$T_e(0) = T_i(0) = T_0. \tag{8}$$

The presence of an external source (laser) violates the equilibrium distribution. In one case, due to radiative losses the concentrations of charged particles in excited states can be lower than the Saha–Boltzmann concentrations and the average charge of the plasma proves to be smaller than the equilibrium charge [3]. In another case, the reverse situation can take place, when the excited states of a particle, whose concentrations are higher than the equilibrium Saha–Boltzmann concentrations at the same temperature, are saturated upon resonance absorption of photons, and the average charge of the plasma is larger than the equilibrium charge [5].

By solving simultaneously the system of kinetic ordinary differential equations (1)–(5) and energy balance equations (6), (7) with initial conditions (8) and a given external energy source, we can obtain new (not Saha–Boltzmann) level populations, which allow us to calculate not only the relative line intensities but also their absolute values.

Note that the description of level population processes and the charge composition of plasmas in the nonequilibrium approximation finds widespread application in the last years [7–14]. A specific feature of the nonequilibrium ionisation of atoms and ions of most chemical elements, in particular, metals is that their energy levels are split and intermixed. Therefore, a great number of excited states (of the order of 10 for each particle) and collision–radiation transitions between them should be taken into account in the description of the kinetics of energy levels [7, 8].

Not pretending to complete citation, we mention among many papers those in which the most typical approaches were proposed. Depending on the aims of the study and chemical elements investigated, the two- [9] and three-level [10–12] kinetic models are often used, which enter, as a rule, as a part into more complicated gas-dynamic [13] or radiative gas-dynamic [14] models. The most complete kinetic model describing the nonequilibrium ionisation of atoms and ions of metals is presented in papers [7, 8]. However, this model neglects photoprocesses. In our paper, the model [7, 8] is supplemented with photoprocesses in laser-radiation and continuum fields.

We used the kinetic nonequilibrium collision–radiation model (1)–(8) to study the optical breakdown in papers [5, 6], where expressions for all kinetic coefficients are presented.

3. Mechanisms of spectral line broadening

The emission of an atom or ion during its transition between the discrete states m and n is not strictly monochromatic due to line broadening effects. The shape of each spectral line is determined by its central core, which is calculated in the collision approximation, and by the line wings broadened by ion fields. In the general case, the line core is described by the Voigt spectral function $S^z_{mn}(\Delta\omega)$, which is a convolution of the Doppler ${}^{D}S^z_{mn}(\Delta\omega)$ and Lorentzian ${}^{L}S^z_{mn}(\Delta\omega)$ contours [15]

$$S^z_{mn}(\Delta\omega) = \int_{-\infty}^{\infty} {}^{L}S^z_{mn}(\Delta\omega)\,{}^{D}S^z_{mn}(\Delta\omega)\,d\omega$$

$$= \frac{a}{\pi^{3/2}\omega_D}\int_{-\infty}^{\infty}\frac{\exp(-y^2)dy}{a^2+[(\Delta\omega/\omega_D)-y]^2}, \qquad (9)$$

where $a = \Delta\omega_L/\Delta\omega_D$; $\Delta\omega = \omega - \omega^0_{mn}$; $\omega^0_{mn} = E_{mn}/\hbar$ is the frequency of the line centre; E_{mn} is the $m-n$ transition energy; $\Delta\omega_D = (\omega_{mn}/c)(2T_i/M)^{1/2}$ [15] is the Doppler broadening; $\Delta\omega_L = \Delta\omega_H + \Delta\omega_N + \Delta\omega_4$ is the Lorentzian broadening determined by a sum of different collision mechanisms; $\Delta\omega_H = (A_n + A_m)/2$ [15] is the natural linewidth; A_n and A_m are the decay probabilities for the n and m levels; $\Delta\omega_N = \pi r_a^2 v_a \sum N^0_m$ [16] is the line broadening caused by neutral particles; $v_a = (2T_i/M_a)^{1/2}$ is the atom velocity; r_a is the atom radius; $\Delta\omega_4$ is the line broadening caused by the electric field of electrons and ions (quadratic Stark effect).

For the spectral lines of non-hydrogen-like atoms, the quadratic Starke effect takes place, at which the line splitting is proportional to the square of the electric-field strength. In the case of adiabatic collisions [15],

$$\Delta\omega_4 = 38.8C_4^{2/3}\left[(v_e^{1/3} + v_i^{1/3})N_e + 2v_i^{1/3}N_i\right], \qquad (10)$$

$$C_4 = \frac{e^4\bar{z}^2}{2m_e\hbar}\left(\sum_{m<n}\frac{f_{mn}}{\omega^2_{mn}} - \sum_{k<m}\frac{f_{km}}{\omega^2_{km}}\right), \qquad (11)$$

where v_e and v_i are the thermal velocities of electrons and ions. The non-adiabaticity of collisions is taken into account with the help of the function $J(\beta)$ [17]:

$$C_{4e} = C_4 J(\beta), \qquad (12)$$

where

$$\beta = \left(f_{mn}\frac{\mathrm{Ry}}{E_{mn}}\right)^{1/2}\frac{E_{mn}}{T_e} \quad (\beta \in [0,\infty])$$

is the dimensionless parameter; f_{mn} is the oscillator strength of the transition; ω_{nm} is the transition frequency; $\bar{z}$ is the plasma charge; and Ry is the Rydberg constant. The parameter $\beta \to \infty$ corresponds to the adiabatic perturbation of levels, and when inelastic collisions dominate, $\beta \to 0$ and $J(\beta) \to 0$.

The collision approximation is valid in the frequency range $\omega_{mn} \ll \Omega_{e,i}$ [17], where $\Omega_{e,i} = v_{e,i}\rho_B^{-1/3}$ are the Weisskopf frequencies for electrons and ions;

$$\rho_B^{-3} = 5.1\times 10^{19}\frac{E^2_{mn}T^{1/2}}{f_{mn}\bar{z}^{5/2}}$$

is the Weisskopf radius; and T is the plasma temperature. In the frequency range $\omega_{mn} \gg \Omega_{e,i}$ the line wings are located, which are broadened by the microfields of ions and are calculated in the nearest neighbour approximation [15]:

$$S^z_{mn}(\Delta\omega) = \pi\frac{C_4^{3/4}}{\Delta\omega^{7/4}}N_i\exp\left(\frac{-1.33C_4^{3/4}}{\Delta\omega^{3/4}}N_i\right). \qquad (13)$$

The central core (9) is jointed with wings (13) in the frequency interval $\omega_{mn} \sim \Omega_i$ by using the cubic spline interpolation. To provide the adequacy of the model, the condition of the applicability of binary approximation $N_{e,i}\rho_B^3 = \varepsilon_{e,i} \ll 1$ should be fulfilled [14].

In a dense hot plasma, where the line broadening is mainly determined by the quadratic Stark effect, the formation of the line shape strongly depends on the method of determining the constant C_4 [18–20]. Usually, its values lie in the range from 10^{-15} to 10^{-12} cm^4 s^{-1}. For comparison, we present the values of C_4 for different elements and different transition wavelengths taken from the literature and the values of C_{4e} calculated from (12) (Table 2). It follows from Table 2 that constants C_4 and C_{4e} can substantially depend on the choice of the number of perturbing levels and spectroscopic data used [21–23].

Table 2.

Element	Transition wavelength/nm	C_{4e}/cm^4 s^{-1}	C_4/cm^4 s^{-1}
Ar I	104.82	6.0×10^{-15}	8.0×10^{-15} [2] 5.9×10^{-15} [18]
Ar I	106.66	5.8×10^{-15}	8.0×10^{-15} [2] 6.2×10^{-15} [18]
Mg I	517.2	1.8×10^{-15}	3.0×10^{-15} [1]
Mg I	518.3	1.8×10^{-15}	3.0×10^{-15} [1]
Na I	616.07	2.3×10^{-13}	3.6×10^{-13} [15]
Na I	819.48	6.8×10^{-13}	1.1×10^{-12} [15]

4. Simulations and analysis of results

4.1 Simulation of spectral line shapes in an optically transparent plasma

The proposed model of broadening of spectral line (9) was tested by analysing the results of two experimental papers [24, 25] in which four lines were studied. The optical transparency was provided in both experiments by the low electron density $N_e < 2\times10^{17}$ cm^{-3}.

In [24], the shape of the 392.0-nm line of the first carbon ion C II was measured by assuming the local thermodynamic equilibrium at the temperature $T = 1.82$ eV and the electron density $N_e = 1.12\times10^{17}$ cm^{-3}. The half-width of this line was 0.6 Å.

Figure 1 shows the shape of the 392.0-nm line of C II calculated by using model (1)–(13). The calculated half-width is 0.56 Å for the same T and N_e as in [24]. The simulation also showed that the line shape is determined by the quadratic Stark effect and the calculated Voigt profile completely coincides with a Lorentzian profile under experimental conditions. The calculated half-width of the line differs from the measured value less than by 7%. Taking into account the error of measuring the electron concentration, this coincidence is acceptable. Figure 2 shows the dependence of the line half-width on the electron density.

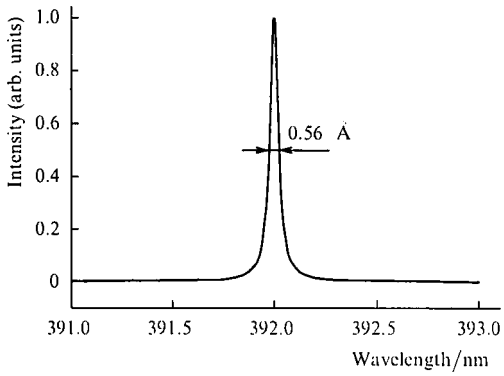

Figure 1. Shape of the 392.0-nm line of the first carbon ion C II for $T = 1.82$ eV and $N_e = 1.12 \times 10^{17}$ cm^{-3}.

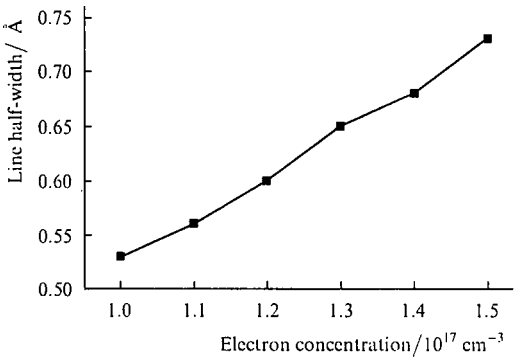

Figure 2. Dependence of the half-width of the 392.0-nm spectral line of the first carbon ion C II on the electron concentration.

The half-widths of the 587.6-nm and 667.8-nm lines of He I in a helium plasma measured by assuming the local thermodynamic equilibrium at the temperature $T = 2-3$ eV are presented in [25]. It was found that the central parts of the lines had a complicated structure due to splitting. The electron concentration was within $(1 - 10) \times 10^{16}$ cm^{-3}. The measured half-widths were 1.2 – 2.0 Å for the 587.6-nm line and 3 – 4 Å for the 667.8-nm line of He I.

The calculated half-widths are 2.0 Å for the 587.6-nm line and 3.4 Å for the 667.8-nm line of He I for $T = 2.5$ eV and $N_e = 10^{17}$ cm^{-3}. The line broadening is predominantly determined by the quadratic Stark effect. The calculated half-widths lie within the interval of the corresponding measured values.

Table 3 presents the parameters corresponding to the collision, quasi-static, and binary approximations.

Therefore, the conditions $\varepsilon_c \ll 1$ and $\varepsilon \ll 1$ are fulfilled for all the three lines, which justifies the use of the binary approximation. Collisions between electrons lead to the broadening of the central parts of the lines in the collision approximation because the inequality $\Delta\omega \ll \Omega_c$ is valid for all the lines. Since the inequality $\Delta\omega < \Omega_i$ is fulfilled, we can assume that the central parts of all the lines are completely broadened in the collision approximation. If the reverse inequality $\Delta\omega > \Omega_i$ is fulfilled, it is necessary to take into account the quasi-static influence of ions on the line centre.

4.2 Simulation of the emission spectrum of a locally equilibrium plasma

The nonequilibrium collision–radiation kinetic model (1)–(8) together with the line broadening model (9)–(13) allows us to calculate the line emission spectrum of a plasma. The simulation was based on the results of experimental paper [26] in which the line emission spectrum of an Ar I plasma was measured. The measurements showed that the plasma was in the local thermodynamic equilibrium with the temperature $T = 2.2 \pm 0.15$ eV and the electron density $N_e = (0.2 - 1.45) \times 10^{17}$ cm^{-3}. The kinetic model of the argon atom contained 25 states and considered 45 transitions between them. The values of temperature and density obtained in [26] were used as initial parameters.

Table 4 presents the calculated (Fig. 3) and experimental relative intensities and half-widths of spectral lines for Ar I. The difference between the experimental and theoretical line shapes can be explained by the error in measuring the constants of quadratic Stark effect, which prove to be understated for the lines 1–3 and 7. This error is caused by several factors. First, the broadening constant was calculated assuming that only the upper level of the transition was perturbed, whereas the lower level remained unperturbed. It follows from this assumption that the constants C_4 of transitions from the same energy state are identical. In this case, the broadening constants will be identical for transitions at 801.48 and 842.46 nm which occur from the state with $\Delta E = 13.095$ eV. Second, the accuracy of calculation of C_4 directly depends on the accuracy of measuring spectroscopic characteristics of

Table 3.

Element	λ/nm	$\Delta\lambda$/Å	$\Delta\omega$/s^{-1}	Ω_e/s^{-1}	Ω_i/s^{-1}	ε_e	ε_i
C II	392.0	0.6	7.4×10^{11}	4.1×10^{15}	2.3×10^{12}	1.2×10^{-6}	1.8×10^{-3}
He I	587.6	2.0	2.2×10^{12}	2.4×10^{15}	5.7×10^{12}	8.6×10^{-6}	9.5×10^{-4}
He I	667.8	3.4	3.6×10^{12}	2.1×10^{15}	5.0×10^{12}	1.3×10^{-5}	1.4×10^{-3}

Table 4.

Number of line in Fig. 3	Transition wavelength/nm	Intensity (arb. units)		Intensity difference (%)	Line half-width/Å		Line half-width difference (%)	C_4/cm^4 s^{-1}
		Experiment	Calculation		Experiment	Calculation		
1	800.61	0.24	0.17	+29.0	1.7	2.3	35.3	1.28×10^{-15}
2	801.48	0.46	0.33	+28.0	1.8	2.3	27.8	1.26×10^{-15}
3	810.37	0.69	0.99	−44.0	–	2.1	–	1.10×10^{-15}
4	811.53	1.0	1.0	0	–	2.6	–	1.62×10^{-15}
5	826.45	0.46	0.46	0	2.2	2.3	4.6	1.29×10^{-15}
6	840.82	0.66	0.62	+6.0	2.2	2.4	9.1	1.41×10^{-15}
7	842.46	0.75	0.69	−8.0	1.9	2.3	21.1	1.26×10^{-15}

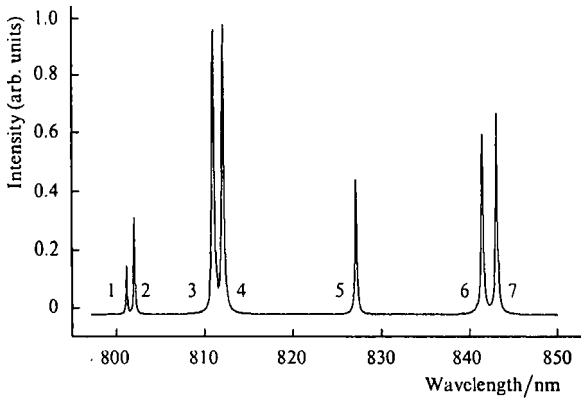

Figure 3. Equilibrium emission spectrum of the argon plasma calculated for $T = 2.2$ eV and $N_e = 1.1 \times 10^{17}$ cm^{-3}.

different transitions. Finally, it is necessary to take into account the number of levels considered, which is always finite in a theoretical model. Table 5 presents the total number k of perturbing levels for Ar I, which were considered in the calculation of the broadening constant.

It follows from Table 5 that the constants C_4 calculated from (11) in the temperature range 1–3 eV can differ approximately twice from those presented in [1, 2, 15, 18]. Because of this, we believe that it is admissible to use a new broadening constant $C_4^* = (0.5 - 2.0)C_4$ in calculations.

The calculation of the line intensities and half-widths with a new constant C_4^* resulted in a better agreement with experimental data. The difference between the theoretical and experimental line intensities does not exceed 20 %, while the maximum difference in the corresponding half-widths proved to be less than 10 %. In the subsequent calculations, we used the constant C_4^* instead of C_4.

4.3 Mathematical simulation of the emission spectrum of a nonequilibrium laser plasma

A number of problems of the laser action such as the optimisation of pulsed laser deposition in manufacturing photoelectric lead-based transducers [27], the optimisation of a UV and soft X-ray radiation source [28–30] based on the radiative cooling of a laser plasma require detailed information on physical processes. Spectroscopic diagnostic is one of the efficient means for solving such problems. A specific property of the laser plasma is its thermodynamic nonequilibrium caused by the release of the laser pulse energy in the electron component, the hydrodynamic expansion of substance and radiation carrying out. The absence of a local thermodynamic equilibrium in the plasma with an arbitrary transparency considerably affects the plasma composition, the degree of its ionisation, and absorption coefficients, which finally strongly complicates calculations of the emission spectrum.

In this section, we studied the dynamics of the emission spectrum of the nonequilibrium plasma produced in the argon atmosphere and determined the main parameters of this spectrum. The laser plasma was produced by irradiating the argon plasma with the initial temperature $T_0 = 0.5$ eV and concentration $N_0 = 2 \times 10^{17}$ cm^{-3} by the 1.06-μm pulses from a neodymium laser. The values of the laser pulse intensity $G \approx 1.1 \times 10^8$ W cm^{-2} and duration $\tau \approx 0.1$ s were selected to provide the passage of the plasma to the equilibrium state with parameters corresponding to the experiment by the pulse end [26].

Figure 4 shows the dynamics of the plasma discharge. The electron component of the argon plasma strongly absorbs laser radiation, resulting in the heating of free electrons up to the temperature $T_e \approx 0.8$ eV by the time $t \approx 5 \times 10^{-5}$ s (Fig. 4c). This leads to the increase in the concentration $N_1 - N_{12}$ of excited states by one–two orders of magnitude (Fig. 4a) and the electron concentration by a factor of 1.3 (Fig. 4b), which is considerably lower than the equilibrium electron concentration $N_e^{Saha}(T_e)$ calculated by the Saha formulas at the electron temperature. Then, the process passes to a slow stage of the optical breakdown development, at which the excited states are gradually populated at virtually constant values of T_e and N_e. For $t = (2 - 4) \times 10^{-2}$ s, a rapid stage of the breakdown is developed, which is caused by the intense ionisation of excited states. The nonequilibrium cascade ionisation is accompanied by a rapid increase in the concentration and energy of free electrons, as well as by a gradual equating of temperatures T_e and T_i. By the instant of time $t \approx 0.5$ s, the system passes to the equilibrium stationary state with the temperature $T_e = T_i \approx 2.35$ eV, the electron concentration $N_e \approx 1.8 \times 10^{17}$ cm^{-3}, and the degree of ionisation close to unity (Fig. 4).

The complex dynamics of a plasma discharge is manifested in the emission spectrum and dominating line broadening mechanisms. Figures 5–10 present the emission spectra and spectral functions $S(\lambda)$ of the nonequilibrium argon plasma corresponding to the four instants $t_1 - t_4$ indicated by the arrows in Fig. 4c.

Figure 5 shows the emission spectrum of the argon plasma obtained at the instant t_1 before the optical breakdown onset ($\nu_{en} \geqslant \nu_{ei}$) for $T_e = 0.88$ eV, $T_i = 0.54$ eV, and $N_e = 1.9 \times 10^{13}$ cm^{-3}. Because the electron density is low, the line broadening is mainly determined by pressure, i.e., by collisions with neutral particles. The amplitudes of spectral functions $S(\lambda)$ are almost the same for all the lines, being

Table 5.

Number of line in Fig. 3	Transition wavelength/nm	C_4/cm^4 s^{-1}	C_4^*/cm^4 s^{-1}	Intensity (arb. units)		Line half-width/Å		k
				Experiment	Calculation	Experiment	Calculation	
1	800.61	1.28×10^{-15}	6.0×10^{-16}	0.24	0.29	1.7	1.7	42
2	801.48	1.26×10^{-15}	7.5×10^{-16}	0.46	0.46	1.8	1.8	46
3	810.37	1.10×10^{-15}	1.8×10^{-15}	0.69	0.69	–	3.0	39
4	811.53	1.62×10^{-15}	1.6×10^{-15}	1.00	1.00	–	2.6	32
5	826.45	1.29×10^{-15}	1.3×10^{-15}	0.46	0.46	2.2	2.3	34
6	840.82	1.41×10^{-15}	1.4×10^{-15}	0.66	0.66	2.2	2.4	37
7	842.46	1.26×10^{-15}	1.4×10^{-15}	0.75	0.72	1.9	2.1	46

equal to $\sim 4 \times 10^{-11}$ s. The excited-state populations are $10^4 - 10^5$ cm^{-3}, so that the radiation power density in lines is $\sim 10^{-6}$ W cm^{-3} (Fig. 5).

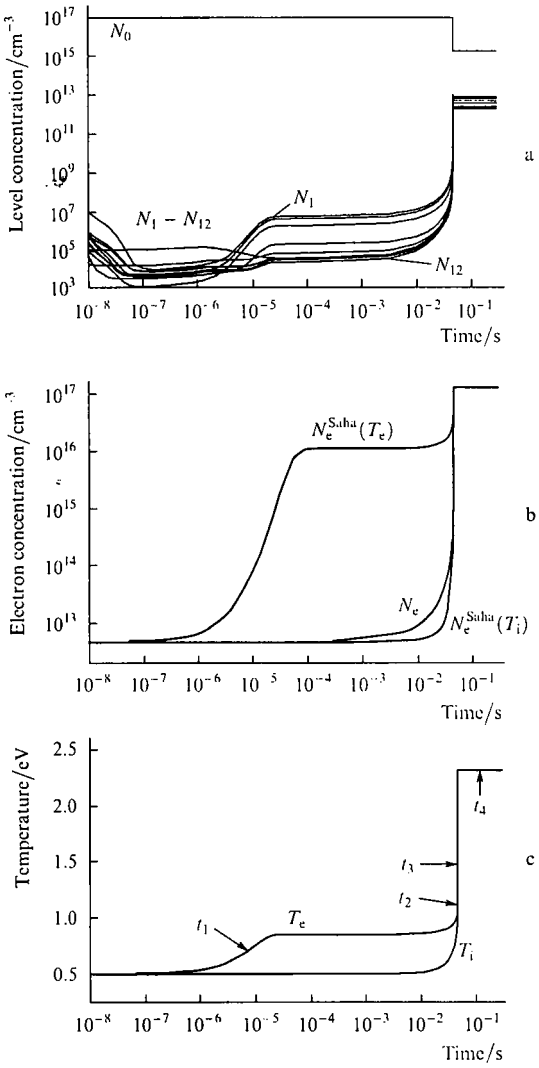

Figure 4. Time dependences of the concentrations of excited states of atoms (a) and electrons (b) and of the electron and ion temperatures (c).

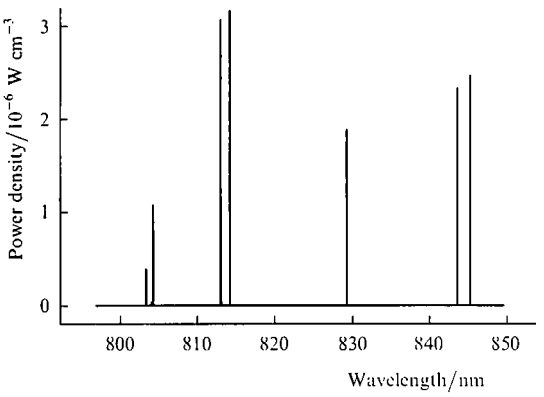

Figure 5. Nonequilibrium spectrum of the argon plasma calculated for $T_e = 0.88$ eV, $T_i = 0.54$ eV, and $N_e = 1.9 \times 10^{13}$ cm^{-3}.

Figure 6 (the instant of time t_2) shows the emission spectrum after the optical breakdown onset ($\nu_{en} \leqslant \nu_{ei}$) for $T_e = 0.95$ eV, $T_i = 0.73$ eV, and $N_e = 8.5 \times 10^{13}$ cm^{-3}. The excited-state populations increase by 20–100 times, resulting in the increase in the power density in lines up to $10^{-5} - 10^{-4}$ W cm^{-3} and in a decrease in the spectral-function amplitude (down to $\sim 3 \times 10^{-11}$ s) caused by the increasing influence of the Stark effect.

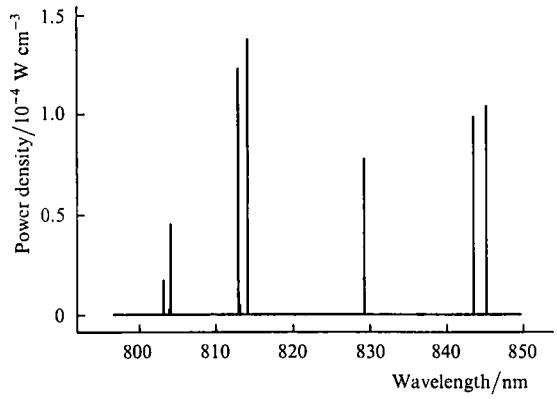

Figure 6. Nonequilibrium spectrum of the argon plasma calculated for $T_e = 0.95$ eV, $T_i = 0.73$ eV, and $N_e = 8.5 \times 10^{13}$ cm^{-3}.

The instant of time t_3 in Fig. 4c corresponds in fact to the establishment of a local thermodynamic equilibrium in the plasma at $T_e = 1.38$ eV, $T_i = 1.35$ eV, and $N_e = 1.4 \times 10^{16}$ cm^{-3}. The broadening of spectral lines is predominantly determined by the Stark effect. For this reason, the radiation power density in the lines continues to grow, achieving 0.1–0.7 W cm^{-3} (Fig. 7) and the amplitudes of spectral functions $S(\lambda)$ decrease by 2–5 times compared to the amplitudes at the instant of time t_2 (Fig. 8).

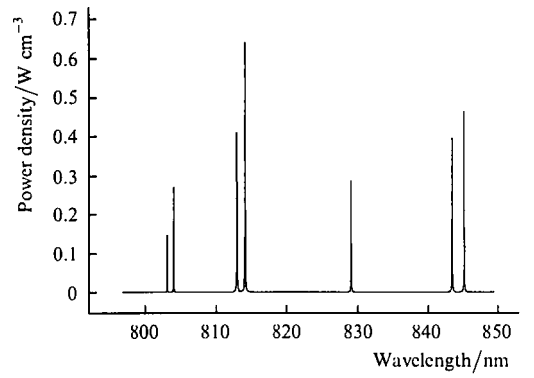

Figure 7. Nonequilibrium spectrum of the argon plasma calculated for $T_e = 1.38$ eV, $T_i = 1.35$ eV, and $N_e = 1.4 \times 10^{16}$ cm^{-3}.

The emission spectrum and spectral functions presented in Figs 9 and 10 correspond to the equilibrium spectrum (at the instant t_4 in Fig. 4c) of the system in the stationary state with the temperature $T = 2.35$ eV and the electron concentration $N_e = 1.8 \times 10^{17}$ cm^{-3}. The equilibrium populations of levels achieve $10^{12} - 10^{13}$ cm^{-3} and the radiation power density is 0.5–1.5 W cm^{-3}.

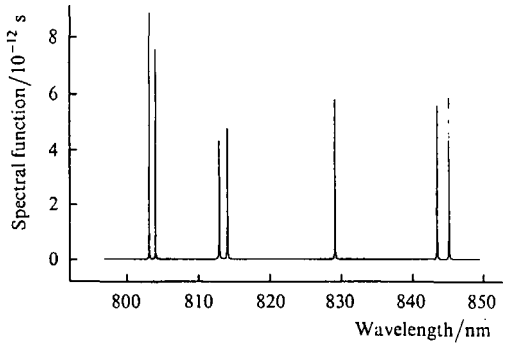

Figure 8. Spectral function $S(\lambda)$ corresponding to the nonequilibrium spectrum in Fig. 7.

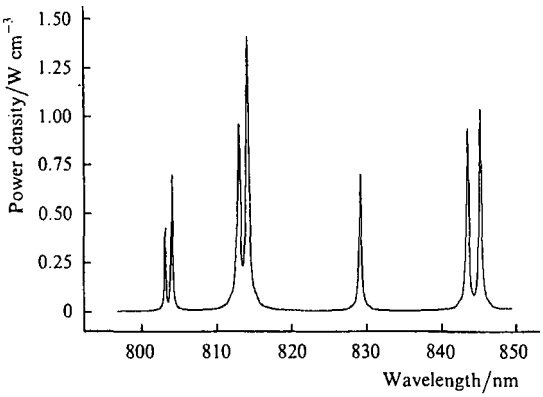

Figure 9. Equilibrium spectrum of the argon plasma calculated for $T_e = 2.35$ eV, and $N_e = 1.8 \times 10^{17}$ cm^{-3}.

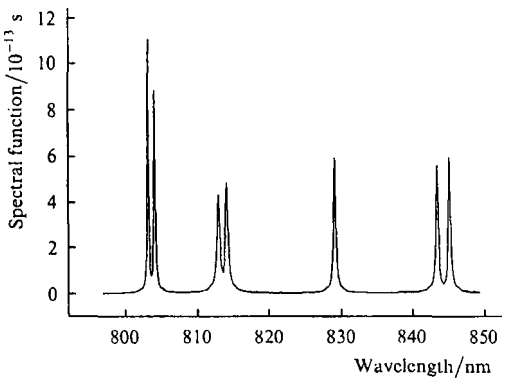

Figure 10. Spectral function $S(\lambda)$ corresponding to the equilibrium spectrum in Fig. 9.

Simulations showed that the maximum radiation power density during the interaction time was achieved before the establishment of the stationary state, when the temperature and electron density have already stabilised, while the level populations achieved the maximum value before their decay (Fig. 4a). The radiation power density in each line in the stationary state decreased by 20 % – 30 % compared to its maximum value.

Table 6 presents the calculated and experimental [26] relative intensities of the emission lines in the equilibrium spectrum. One can see that the relative intensities are in agreement with an acceptable accuracy.

Table 6.

Number of line in Fig.3	Transition wavelength/nm	Intensity (arb. units)	
		Experiment [26]	Simulation
1	800.61	0.29	0.30
2	801.48	0.46	0.49
3	810.37	0.69	0.68
4	811.53	1.00	1.00
5	826.45	0.46	0.50
6	840.82	0.66	0.67
7	842.46	0.72	0.73

Thus, the emission spectra of the equilibrium and nonequilibrium plasma can strongly differ from each other, even if they correspond to the same temperatures and the same initial concentrations of particles.

5. Conclusions

We have calculated the line emission spectrum of the nonequilibrium argon plasma and developed a complete collision–radiation kinetic model describing processes of the nonequilibrium population of levels taking into account the main line broadening mechanisms and nonequilibrium ionisation of atoms and ions. The kinetic model was supplemented with the energy balance equations for electrons and atoms.

This physicomathematical model was tested based on experiments in which the parameters of spectral lines of different elements (He, C, Ar) were measured under the conditions of a local thermodynamic equilibrium. A comparison of the results of simulations and measurements has demonstrated acceptable agreement between the calculated and experimental linewidths and line shapes.

The mathematical simulation of the optical-breakdown argon plasma has shown that the intensities of nonequilibrium line spectra can be noticeably (by several times) lower than those of equilibrium spectra. Due to the use of shorter and higher-power laser pulses, the nonequilibrium emission spectrum differs from the equilibrium spectrum not only quantitatively but also qualitatively, i.e., the spectra contain the different number of lines.

The results obtained in the paper can be used to substantiate physicomathematical models proposed for simulations of nonequilibrium dynamic situations in plasma discharges and to calculate the corresponding line spectra.

Acknowledgements. This work was supported by the Russian Foundation for Basic Research (Grant No 04-01-00701).

References

1. Gray D. *Observation and Analysis of Stellar Atmospheres* (Moscow: Mir, 1980).
2. Griem H.R. *Spectral Line Broadening by Plasmas* (New York: Academic Press,1974; Moscow: Mir, 1978).
3. Gudzenko L.I., Yakovlenko S.I. *Plazmennye lazery* (Plasma Lasers) (Moscow: Atomizdat, 1978).
4. Stupitskii E.L., Lyubchenko O.S., Khudaverdyan A.M. *Kvantovaya Elektron.*, **12**, 1038 (1985) [*Sov. J. Quantum Electron.*, **15**, 682 (1985)].
5. Mazhukin V.I., Nikiforov M.G., Nosov V.V. *Matemat. Model.*, **4**, 3 (2002).